Exergy in near-field electromagnetic heat transfer

Hideo Iizuka, and Shanhui Fan

Citation: Journal of Applied Physics **122**, 124306 (2017); doi: 10.1063/1.5004662
View online: http://dx.doi.org/10.1063/1.5004662
View Table of Contents: http://aip.scitation.org/toc/jap/122/12
Published by the American Institute of Physics

Exergy in near-field electromagnetic heat transfer

Hideo Iizuka[1,a)] and Shanhui Fan[2,b)]
[1]*Toyota Research Institute of North America, Toyota Motor North America, Ann Arbor, Michigan 48105, USA*
[2]*Department of Electrical Engineering, Ginzton Laboratory, Stanford University, Stanford, California 94305, USA*

(Received 24 May 2017; accepted 14 September 2017; published online 29 September 2017)

The maximum amount of usable work extractable from a given radiative heat flow defines the exergy. It was recently noted that the exergy in near-field radiative heat transfer can exceed that in the far-field. Here, we derive a closed form formula of exergy in the near-field heat transfer between two parallel surfaces. This formula reveals that, for a given resonant frequency, the maximum exergy depends critically on the resonant linewidth, and there exists an optimal choice of the linewidth that maximizes the exergy. Guided by the analytical result, we show numerically that with a proper choice of doping concentration, the heat flow between two properly designed SiC-coated heavily doped silicon regions can possess exergy that is significantly higher compared to the heat flow between two SiC regions where the heat flow is carried out by phonon-polaritons. Our work indicates significant opportunities for either controlling material properties or enhancing the fundamental potential for near-field heat transfer in thermal energy conversion through the approach of meta-material engineering. *Published by AIP Publishing.* https://doi.org/10.1063/1.5004662

I. INTRODUCTION

Radiative heat flow carries both energy and entropy. As a result, the maximum amount of usable work extractable from a given radiative heat flow, which defines the exergy, is less than the energy carried by the heat flow. The ratio between the exergy and the energy carried by the heat flow defines the maximum efficiency at which the heat flow can be converted into work. In the far-field regime of radiative heat transfer, the analysis of exergy has led to the establishment of the Landsberg limit,[1] which plays a major role in the understanding of the theoretical limit for the efficiency of thermal energy conversion.[2–4] In the near-field regime, there have been several recent analyses of the exergy contained in near-field heat flow.[5–7] In particular, in Refs. 6 and 7, it was shown that both the exergy in the near-field heat flow and the maximum efficiency through which the heat flow can be converted into work can exceed those in the far-field heat transfer. References 6 and 7 therefore pointed to an important fundamental opportunity that near-field heat transfer can play a role in thermal energy harvesting[8–24] in addition to the enhancement of heat flow.[25–38]

Reference 6 provided analytical results for both the exergy and the maximum conversion efficiency for the near-field heat flow between two materials having a photon-polariton response. In these systems, the near-field heat transfer has a narrow spectrum centered at a resonant frequency ω_0. Reference 6 has shown that having such a narrow spectrum is important in order to have a high efficiency beyond the Landsberg limit. Also, as the resonant frequency ω_0 increases, the maximum efficiency increases but the heat flow decreases. On the other hand, in addition to efficiency considerations, it is also important to achieve the maximum exergy that can possibly be obtained. Also, as a significant opportunity, with the development of meta-materials,[39,40] and with the use of materials such as heavily doped silicon,[41] one now in principle has significant control over both the resonant frequency and the linewidth γ of the resonance in the near-field heat transfer. It is therefore of interest to provide a more systematic study on the dependency of the exergy on various system parameters.

In this paper, building upon our previous work in Ref. 42, we provide a simpler closed-form formula of exergy in the near-field heat transfer. This formula reveals that, for a given resonant frequency ω_0, the maximum efficiency is largely independent of the resonant linewidth γ. On the other hand, the maximum exergy itself depends critically on the resonant linewidth γ, and there exists an optimal choice of the linewidth γ that maximizes the exergy. Guided by the analytical result, we show numerically that with a proper choice of doping concentration of heavily doped silicon and the use of SiC films, thermal bodies can have parameters that approach such optima, and as a result, the heat flow between two properly designed SiC-coated heavily doped silicon regions can possess exergy that is significantly higher compared to a typical phonon-polariton system with similar resonant frequencies. Our work provides significant opportunities for either controlling material or meta-material properties or enhancing the fundamental potential for near-field heat transfer in thermal energy conversion.

II. ANALYTICAL STUDIES OF EXERGY

A. Device geometry

We consider a geometry consisting of parallel plates separated by a vacuum gap size d, as shown in Fig. 1. The two plates have different temperatures T_1 and T_2 ($T_1 > T_2$).

a)hideo.iizuka@toyota.com
b)shanhui@stanford.edu

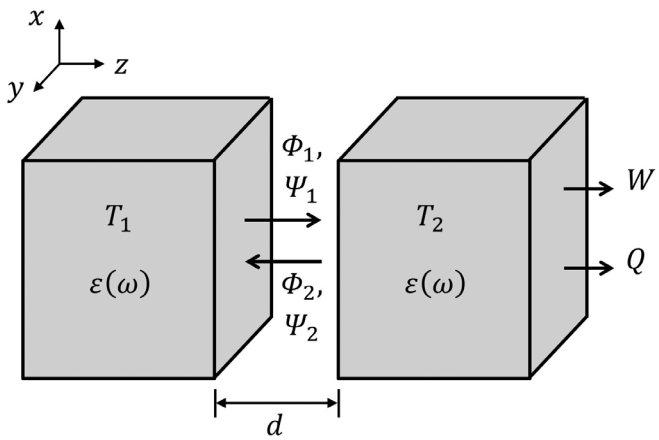

FIG. 1. Geometry of parallel plates with temperatures T_1 and T_2 $(T_1 > T_2)$ for obtaining exergy in the near-field heat transfer process. Φ and Ψ denote the energy and entropy flow, respectively.

We assume that each plate has its permittivity described by the Drude model,

$$\varepsilon(\omega) = \varepsilon_\infty - \frac{{\omega_p}^2}{\omega(\omega + i\gamma)}, \tag{1}$$

where ε_∞ and ω_p are the permittivity at infinite frequency and the plasma frequency, respectively. In this geometry, when we are in the near-field regime and the gap size is smaller than the characteristic thermal wavelength, the p-polarized evanescent waves dominantly contribute to the heat transfer due to the existence of plasmon or phonon polariton excitations in this polarization. Consequently, the net energy flux Φ and the entropy flux Ψ transferred from one plate to the other are given by[7]

$$\Phi = \Phi_1 - \Phi_2, \tag{2}$$

$$\Psi = \Psi_1 - \Psi_2, \tag{3}$$

where

$$\Phi_i = \int_{k_0}^{\infty} \frac{\beta d\beta}{2\pi} \int_0^{\infty} \frac{d\omega}{2\pi} \frac{4\{Im[r(\omega,\beta)]\}^2 e^{-2\kappa_0 d}}{|1 - r(\omega,\beta)^2 e^{-2\kappa_0 d}|^2} \hbar\omega n(\omega, T_i), \tag{4}$$

$$\Psi_i = \int_{k_0}^{\infty} \frac{\beta d\beta}{2\pi} \int_0^{\infty} \frac{d\omega}{2\pi} \frac{4\{Im[r(\omega,\beta)]\}^2 e^{-2\kappa_0 d}}{|1 - r(\omega,\beta)^2 e^{-2\kappa_0 d}|^2} k_B F(\omega, T_i), \tag{5}$$

with $i = 1, 2$ labelling the two plates. Here, $\hbar$ and k_B are the reduced Planck constant and the Boltzmann constant, respectively. $n(\omega, T)$ and $F(\omega, T)$ denote the number of photons and the entropy, respectively, in a single optical mode with a frequency ω maintained at a temperature T, and they have the following forms:

$$n(\omega, T) = \left(e^{\frac{\hbar\omega}{k_B T}} - 1\right)^{-1}, \tag{6}$$

$$F(\omega, T) = [1 + n(\omega, T)]ln[1 + n(\omega, T)] - n(\omega, T)ln[n(\omega, T)], \tag{7}$$

β and $r(\omega, \beta)$ are the lateral wavenumber and the corresponding Fresnel reflection coefficient of the p-polarized evanescent waves at the vacuum-plate interface. The normal wavenumber in the vacuum has the form of $\kappa_0 = \sqrt{\beta^2 - {k_0}^2}$ $(k_0 < \beta)$, where k_0 is the free space wavenumber. We have ignored the contributions from the s-polarization and consider only the evanescent wave. This approximation is well justified in the near-field regime for this system. The exergy and the conversion efficiency in the system of Fig. 1 are defined as

$$W = (\Phi_1 - \Phi_2) - T_2(\Psi_1 - \Psi_2), \tag{8}$$

$$\eta = \frac{W}{\Phi_1} = \left(1 - \frac{\Phi_2}{\Phi_1}\right) - \frac{T_2(\Psi_1 - \Psi_2)}{\Phi_1}. \tag{9}$$

B. Analytical derivation of optimum exergy and material response

The exergy and maximum efficiency of the system in Fig. 1 can be evaluated by numerical integration of the formulas presented in Sec. II A. On the other hand, in order to gain a deeper insight into how various parameters can be controlled to optimize the exergy and maximum efficiency, it is desirable to have a simpler analytical formula. In this section, we derive an analytical form of the exergy for the system in Fig. 1, building upon some of our previous works in Ref. 42. In the lossless case, the surface resonance frequency is given by

$$\omega_0 = \frac{\omega_p}{\sqrt{\varepsilon_\infty + 1}}. \tag{10}$$

In the near-field heat transfer between parallel plates, the heat transfer via p-polarized evanescent waves is sharply peaked at the surface resonance ω_0. This property is used in Ref. 42 to arrive at a closed form formula. In Ref. 42, in order to evaluate the integrals in Eq. (4), a contour integration is first carried out in the complex ω plane. The resulting expression contains contributions from poles that correspond to the surface polariton resonances in the parallel-plate structure. Then, the β integration is carried out where one introduces a cut-off wavenumber. As a result, the energy flux of Eq. (4) is approximately expressed by the closed form formula[42]

$$\Phi_i = \sigma(\omega_0, \varepsilon_\infty, \gamma, d)\hbar\omega_0 n(\omega_0, T_i), \tag{11}$$

where

$$\sigma(\omega_0, \varepsilon_\infty, \gamma, d) = \frac{\gamma}{8\pi d^2}\left\{ln\left[1 + \frac{2\omega_0}{(\varepsilon_\infty + 1)\gamma}\right]\right\}^2. \tag{12}$$

Likewise, we apply the derivation process in Ref. 42 to the entropy flux of Eq. (5) and now have the closed form formula of the entropy flux as

$$\Psi_i = \sigma(\omega_0, \varepsilon_\infty, \gamma, d)k_B F(\omega_0, T_i). \tag{13}$$

Substituting Eqs. (11) and (13) into Eq. (8) and using the formulas for $n(\omega, T)$ and $F(\omega, T)$ in Eqs. (6) and (7), we have

$$W(\omega_0, \varepsilon_\infty, \gamma, d, T_1, T_2) = \sigma(\omega_0, \varepsilon_\infty, \gamma, d)W_s(\omega_0, T_1, T_2), \tag{14}$$

where

$$W_s(\omega_0, T_1, T_2) = \left(1 - \frac{T_2}{T_1}\right)\hbar\omega_0[1 + n(\omega_0, T_1)] - k_B T_2 ln\left[\frac{n(\omega_0, T_1)}{n(\omega_0, T_2)}\right]. \quad (15)$$

The results here enable us to analytically study the dependencies of exergy on the parameters ε_∞, ω_p, and γ of the Drude model in Eq. (1). Optimizing the exergy W with respect to the linewidth γ, the condition $\frac{\partial W}{\partial \gamma} = 0$ gives

$$\gamma = \frac{C_1\omega_0}{\varepsilon_\infty + 1} \approx \frac{\omega_0}{2(\varepsilon_\infty + 1)}, \quad (16)$$

where $C_1 \approx 0.51$ is the solution of $ln\left(1 + \frac{2}{C_1}\right) - \frac{4}{C_1+2} = 0$. Equation (16) indicates the existence of an optimum choice of the linewidth of a material for maximizing the exergy. With this choice of γ, we observe that the imaginary part of the permittivity at resonance is $Im[\varepsilon(\omega_0)] = \frac{(\varepsilon_\infty+1)\gamma}{\omega_0} = 0.5$. We will use this observation in the numerical design of systems that optimize the exergy. The prefactor σ in Eq. (14) for the maximum W is written as

$$\sigma\left(\omega_0, \varepsilon_\infty, \gamma = \frac{\omega_0}{2(\varepsilon_\infty + 1)}, d\right) = \frac{(ln5)^2\omega_0}{16(\varepsilon_\infty + 1)\pi d^2}. \quad (17)$$

As a result, we obtain the closed form of the optimized exergy for the system in Fig. 1 from Eqs. (14) and (17) as

$$W\left(\omega_0, \varepsilon_\infty, \gamma = \frac{\omega_0}{2(\varepsilon_\infty + 1)}, d, T_1, T_2\right) = \frac{(ln5)^2\omega_0}{16(\varepsilon_\infty + 1)\pi d^2} W_s(\omega_0, T_1, T_2), \quad (18)$$

where to maximize the exergy W, ω_0 satisfies

$$W_s(\omega_0, T_1, T_2) + \omega_0 \frac{\partial W_s(\omega_0, T_1, T_2)}{\partial \omega_0} = 0. \quad (19)$$

Optimizing W with respect to ε_∞, we see that W is maximized with $\varepsilon_\infty = 1$. Substituting $\varepsilon_\infty = 1$ into Eq. (18), the maximum W is obtained as

$$W\left(\omega_0, \varepsilon_\infty = 1, \gamma = \frac{\omega_0}{4}, d, T_1, T_2\right) = \frac{(ln5)^2\omega_0}{32\pi d^2} W_s(\omega_0, T_1, T_2). \quad (20)$$

With these analytical results, one can determine the optimal material parameters that maximize the exergy, when the temperatures T_1 and T_2 of the two plates, as well as the distance d between the two plates, are given.

On the other hand, substituting Eqs. (11) and (13) into Eq. (9), the conversion efficiency into work from the heat flow in such a parallel plate system is given by

$$\eta(\omega_0, T_1, T_2) = \left(1 - \frac{T_2}{T_1}\right) - \frac{1}{n(\omega_0, T_1)} \frac{ln\left[\frac{1 + n(\omega_0, T_1)}{1 + n(\omega_0, T_2)}\right]}{ln\left[\frac{1 + n(\omega_0, T_1)}{n(\omega_0, T_1)}\right]} \frac{T_2}{T_1}. \quad (21)$$

We note that the efficiency of Eq. (21) depends only on $\omega_0 = \frac{\omega_p}{\sqrt{\varepsilon_\infty+1}}$ and does not depend on resonant linewidth γ. This result on efficiency agrees with Ref. 6. On the other hand, Ref. 6 did not give a condition for maximizing the exergy itself.

III. RESULTS

Motivated by the analytical results in Sec. II, in this section, we present several numerical studies. We first present a numerical validation of the analytical formulas shown above and discuss how various parameters influence the magnitude of exergy. Using the analytical results as the guidance, we then show that the exergy in the near-field heat transfer between two heavily doped silicon regions can be optimized by controlling the doping level. Moreover, by placing a thin film of SiC on top of the heavily doped region, we can obtain significant further enhancement of the exergy. Throughout this section, unless otherwise mentioned, we use temperatures $T_1 = 400\,K$ and $T_2 = 300\,K$ of the two bodies and a $d = 10\,\text{nm}$ distance as the size of the vacuum gap between the parallel surfaces. We use material permittivities of silicon and SiC at room temperature since there is little temperature-dependence of permittivities of silicon[43] and SiC[44,45] in the temperature range of our investigation.

The optimum frequency ω_0 for maximizing the exergy is only dependent on temperatures T_1 and T_2, as seen in Eq. (19). Figure 2 shows the behavior of ω_0 as a function of T_1 with $T_2 = 300K$ fixed. We see that the frequency ω_0 monotonically increases with T_1. The analytical result (blue solid line) obtained from Eq. (19) reasonably agrees with the frequencies when the exergy is maximized with variations of ω_0, γ, and ε_∞ in the fluctuational electrodynamics results (blue circles) obtained by evaluating Eqs. (1)–(8) numerically. The conditions for maximizing the exergy have similarities and differences as compared with the conditions for maximizing energy. The optimal frequencies for maximizing the exergy (blue solid line) and the energy (green dashed line) are different, as seen in the comparison of the two lines in Fig. 2, where the optimal frequency for maximizing the energy is given by replacing $W_s(\omega_0, T_1, T_2)$ with $\hbar\omega_0[n(\omega_0, T_1) - n(\omega_0, T_2)]$ in Eq. (19). On the other hand, the conditions of $\varepsilon_\infty = 1$ and $\gamma = \omega_0/4$, which are associated with the prefactor σ in Eqs. (14) and (17), are the same for maximizing both the exergy and the energy.

Figures 3(a) and 3(b) show the dependencies of exergy W on ω_0, γ, and ε_∞. We consider two cases of $\varepsilon_\infty = 11.7$ and $\varepsilon_\infty = 1$. Each case has its optimum parameters of ω_0 and γ as provided in the caption of Fig. 3. In Fig. 3(a), we keep γ fixed at the optimal values and vary ω_0. In Fig. 3(b), we keep ω_0 fixed at the optimal value and vary γ. In both cases, the numerical results from direct the fluctuational

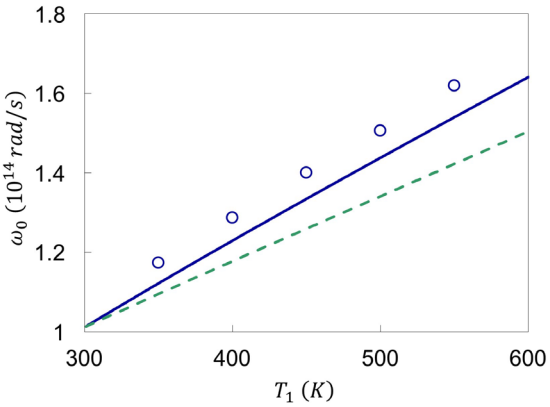

FIG. 2. Optimum frequency ω_0 for maximizing exergy as a function of temperature T_1 with $T_2 = 300\,\mathrm{K}$ fixed. The blue solid line represents the analytical result obtained from Eq. (19). Blue circles are obtained when exergy is maximized in the fluctuational electrodynamic results [Eqs. (1)–(8)] with variations of ω_0, γ, and ε_∞. The distance between two plates is set at $d = 10nm$. The green dashed line represents the optimum frequency for energy that is obtained with the replacement of $W_s(\omega_0, T_1, T_2)$ by $\hbar\omega_0[n(\omega_0, T_1) - n(\omega_0, T_2)]$ in Eq. (19).

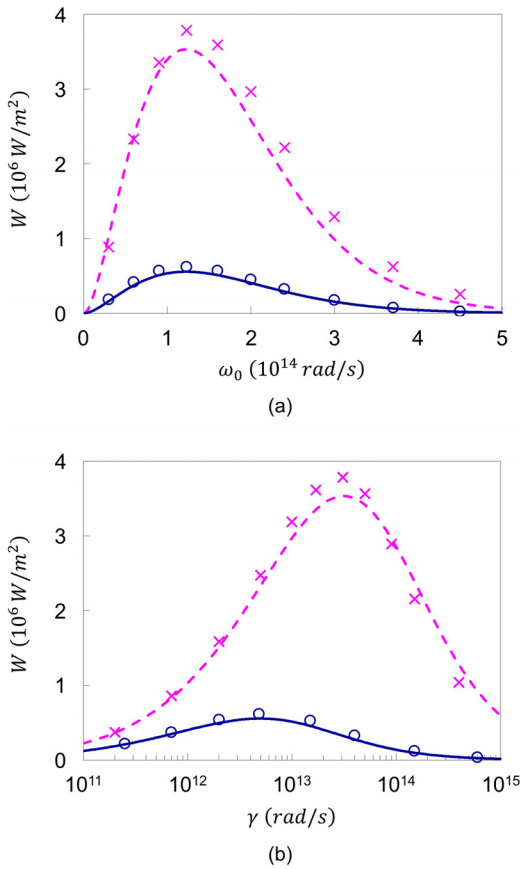

FIG. 3. Exergy as a function of (a) the resonant frequency ω_0 and (b) the resonant linewidth γ with $\varepsilon_\infty = 11.7$ (blue solid lines and circles) and $\varepsilon_\infty = 1$ (pink dashed lines and crosses). The maximum exergy is obtained with $\omega_0 = 1.23 \times 10^{14}\,\mathrm{rad/s}$ and $\gamma = 4.8 \times 10^{12}\,\mathrm{rad/s}$ ($\gamma = 3.1 \times 10^{13}\,\mathrm{rad/s}$) for $\varepsilon_\infty = 11.7$ ($\varepsilon_\infty = 1$). In (a) we keep γ fixed at the optimal values and vary ω_0. In (b), we keep ω_0 fixed at the optimal value and vary γ. The lines represent the analytical results [Eq. (18) for $\varepsilon_\infty = 11.7$ and Eq. (20) for $\varepsilon_\infty = 1$]. The symbols represent the numerical results obtained by the fluctuational electrodynamics [Eqs. (1)–(8)]. Other parameters are $T_1 = 400\,\mathrm{K}$, $T_2 = 300\,\mathrm{K}$, and $d = 10\,\mathrm{nm}$.

electrodynamics equation agree quite well with the analytical results of Eqs. (18) and (20).

From Eq. (15), we see that the exergy W_s of a single optical mode decreases with the increasing frequency ω_0. [Note that the photon number $n(\omega_0, T)$ decreases with ω_0.] On the other hand, the prefactor σ [Eq. (17)], which provides a measure of an effective number of modes that contribute to the heat transfer, increases linearly with ω_0. The two competing trends of W_s and σ result in an optimal of ω_0 that maximizes the exergy in Fig. 3(a). In the dependency of W on γ in Fig. 3(b), W is maximized when the material permittivity has $Im[\varepsilon(\omega_0)] = 0.5$. Regarding the dependency on ε_∞, W is reduced as ε_∞ increases from unity in Figs. 3(a) and 3(b), as can be seen in Eq. (18).

Guided by the discussions above on how various parameters control the magnitude of exergy, we now present a design study of geometries with the aim of maximizing exergy. In general, aside from choosing a different material, it is difficult to strongly influence ε_∞, and therefore, we focus primarily on the mechanism that influences the resonant frequency ω_0 and linewidth γ. As a first example, we choose heavily doped silicon[41] since in the wavelength range, its dielectric function can be strongly tuned by changing the carrier concentration. In Fig. 4(a), we plot the exergy W in this system as a function of the doping concentration N_d, taking the permittivity from Ref. 41, where ω_p and γ are determined from N_d with $\varepsilon_\infty = 11.7$ fixed, using both the analytical formula of Eq. (18) and the direct fluctuational electrodynamics calculation. Again, the two calculations show good agreement. In the fluctuational electrodynamic calculations, the exergy maximizes with a choice of $N_d = 3.1 \times 10^{19}\,\mathrm{cm}^{-3}$, which agrees quite well with the analytical formula that predicts $N_d = 2.5 \times 10^{19}\,\mathrm{cm}^{-3}$. The strong dependency of the exergy as a function of N_d points to the importance of choosing the right material parameters in order to maximize the exergy.

As noted in the discussions in Sec. II, to maximize the exergy, one needs to simultaneously control both parameters ω_0 and γ. For the heavily doped silicon, we have only a single control parameter that is the doping concentration N_d. Using heavily doped silicon alone therefore, we do not have enough degree of freedom to approach the theoretical maximum of exergy. To see this, we plot ω_0 and $Im[\varepsilon(\omega_0)] = \frac{(\varepsilon_\infty+1)\gamma}{\omega_0}$ as a function of the doping concentration N_d in Figs. 4(b) and 4(c). We see in Fig. 4(b) that the optimal doping concentration of $N_d = 2.5 \times 10^{19}\,\mathrm{cm}^{-3}$ corresponds to $\omega_p = 5.42 \times 10^{14}\,\mathrm{rad/s}$ and therefore a resonant frequency of $\omega_0 = 1.52 \times 10^{14}\,\mathrm{rad/s}$, which is quite close to the optimal frequency of $\omega_0 = 1.23 \times 10^{14}\,\mathrm{rad/s}$. However, at such a doping concentration, the damping rate of $\gamma = 7 \times 10^{13}\,\mathrm{rad/s}$ is far from the optimal rate of $\gamma = 4.8 \times 10^{12}\,\mathrm{rad/s}$. As an alternative indication, the imaginary part of the permittivity of doped silicon is far larger than the optimum value of $Im[\varepsilon(\omega_0)] = 0.5$, as shown in Fig. 4(c). For the purpose of maximizing exergy, the material loss of heavily doped silicon is too large.

Based on the above analysis, one strategy to further maximize the exergy is to combine heavily doped silicon

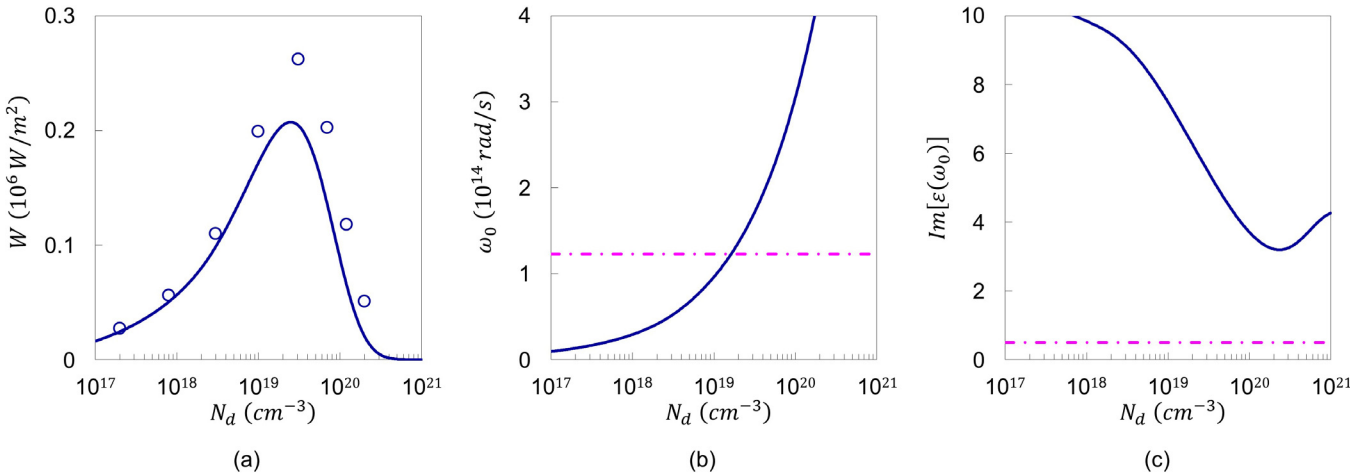

FIG. 4. (a) Exergy W in near-field heat transfer between heavily doped silicon plates as a function of the doping concentration N_d. The curve represents the analytical result [Eq. (18)], and the circles represent the numerical results obtained by the fluctuational electrodynamics [Eqs. (1)–(8)]. (b) Resonant frequency ω_0 and (c) imaginary part of the permittivity $Im[\varepsilon(\omega_0)] = \frac{(\varepsilon_\infty+1)\gamma}{\omega_0}$ as a function of N_d are presented by the solid lines. The horizontal dashed-dotted lines represent the optimum values of $\omega_0 = 1.23 \times 10^{14}$rad/s in (b) and $Im[\varepsilon(\omega_0)] = 0.5$ in (c).

with another material that has lower loss. To implement this strategy, we consider SiC, a typical phonon-polariton material, which has a permittivity of $\varepsilon(\omega) = \varepsilon_\infty \frac{\omega_{LO}{}^2 - \omega^2 - i\gamma\omega}{\omega_{TO}{}^2 - \omega^2 - i\gamma\omega}$, with parameters of $\varepsilon_\infty = 6.7$, $\omega_{LO} = 1.83 \times 10^{14}$ rad/s, $\omega_{TO} = 1.49 \times 10^{14}$ rad/s, and $\gamma = 8.97 \times 10^{11}$ rad/s in Ref. 27. At its surface phonon-polariton frequency, SiC has a permittivity with an imaginary part of $Im[\varepsilon(\omega_0)] \approx 0.13$ that is less than 0.5. By combining heavily doped silicon with SiC then, we expect that the exergy can further increase. We therefore consider the system shown in Fig. 5(a) consisting of a heavily doped silicon coated with SiC. We select $N_d = 3.1 \times 10^{19}$cm^{-3} for the doped silicon such that $\omega_p = 6.06 \times 10^{14}$ rad/s, and therefore, the heavily doped silicon has the resonant frequency of $\omega_0 = 1.7 \times 10^{14}$ rad/s, which is almost the same as that of SiC at 1.79×10^{14} rad/s. Such a choice of N_d reduces the reflection of evanescent waves at the doped silicon-SiC interface because the permittivities of silicon and SiC approximately match each other. As a result, both materials contribute to the heat transfer significantly.

Figure 6 shows the exergy of the SiC-coated doped silicon system as a function of the thickness t of the SiC film. The exergy is 1.5 times and 2 times larger as compared to the doped silicon plate system ($t = 0$) and the SiC plate system (indicated at the right-hand side of Fig. 6 which corresponds to the $t \to \infty$ limit), respectively. The exergy slowly varies as a function of coating thickness. The enhancement effect here is therefore robust with respect to the variation in the layer thickness of SiC. At the optimal SiC thickness, the numerically calculated exergy is about $0.39 \times 10^6 W/m^2$, as compared to the upper bound of exergy of $0.56 \times 10^6 W/m^2$ [Fig. 5(b)], as determined using $\varepsilon_\infty = 11.7$ [Eq. (18)]. The simple geometry as discussed here therefore allows one to approach the upper bound. In this calculation, we have used the reflection coefficient $\tilde{r}$ for the SiC-coated doped silicon plate from the vacuum gap as,

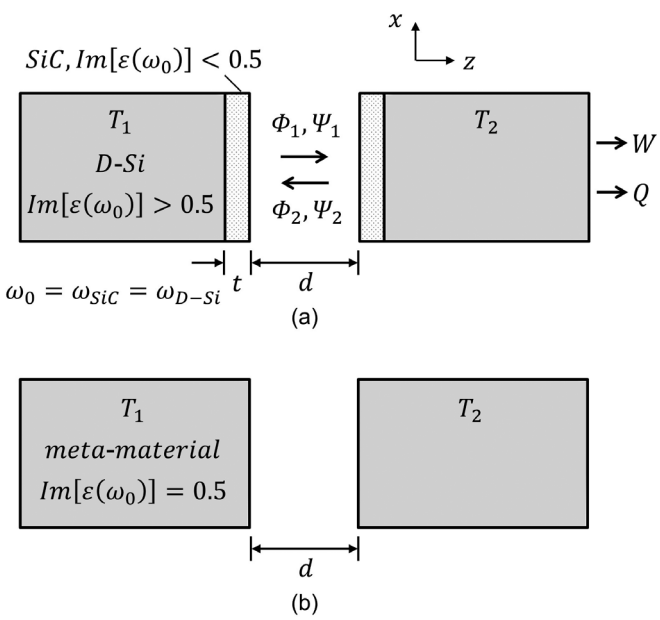

FIG. 5. Schematics of (a) a SiC-coated heavily doped silicon system for the enhancement of exergy and (b) the optimum material system.

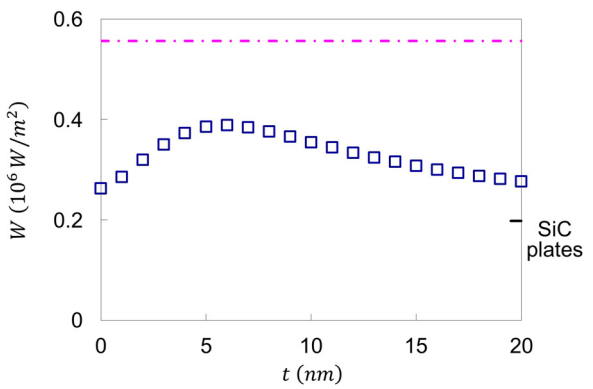

FIG. 6. Exergy (squares) as a function of the thickness of the SiC film in Fig. 5(a). A doping concentration of $N_d = 3.1 \times 10^{19} cm^{-3}$ is selected. The exergy is represented by the square at $t = 0$ in the heavily doped silicon plate system and at the right vertical axis for the SiC plate system. The horizontal dashed-dotted line represents the upper bound of exergy with $\varepsilon_\infty = 11.7$ [Eq. (18)].

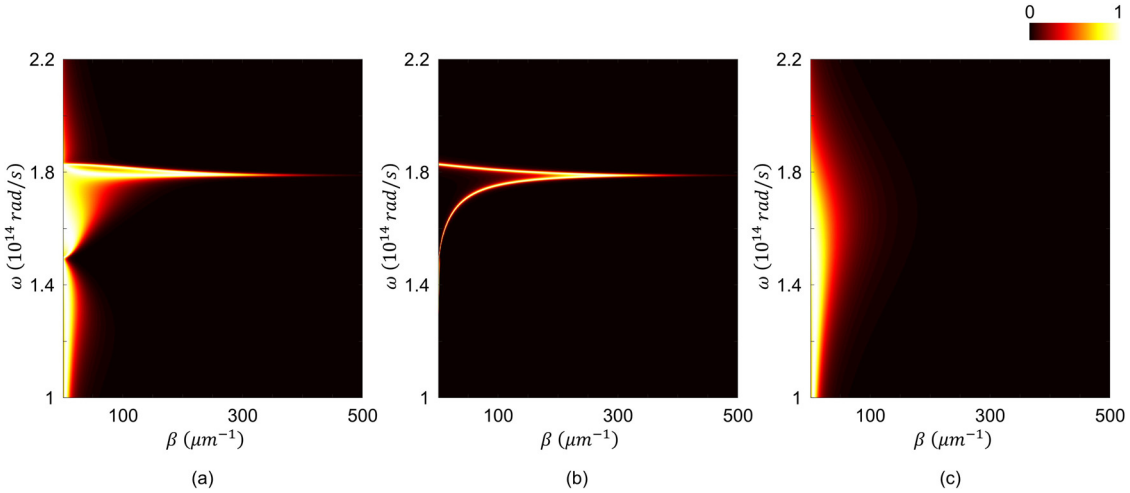

FIG. 7. Normalized exchange functions of (a) the SiC-coated heavily doped silicon system ($N_d = 3.1 \times 10^{19}\text{cm}^{-3}$; $t = 6\,\text{nm}$), (b) SiC system, and (c) heavily doped silicon system ($N_d = 3.1 \times 10^{19}\,\text{cm}^{-3}$).

$$\tilde{r}(\omega,\beta) = \frac{r_{01} + r_{13}e^{-2\kappa_1 t}}{1 - r_{10}r_{13}e^{-2\kappa_1 t}}, \tag{22}$$

where r_{ij} is the Fresnel reflection coefficient of the p-polarized evanescent wave at the interface between i and j media and $i = 0,\ 1$, or 3 labels the vacuum, the SiC film, and the doped silicon plate. κ_1 denotes the normal wavenumber in the SiC film.

At the optimal SiC thickness, both SiC and heavily doped silicon contribute significantly to the heat transfer. In Fig. 7(a), we plot the normalized exchange function $Z(\omega,\beta) \equiv \frac{4\left\{Im[r(\omega,\beta)]\right\}^2 e^{-2\kappa_0 d}}{\left|1-r(\omega,\beta)^2 e^{-2\kappa_0 d}\right|^2}$ in the integrand in Eqs. (4) and (5), as functions of frequency and wavevector for the system of heavily doped silicon with a SiC coating. As a comparison, in Figs. 7(b) and 7(c), we plot the exchange function for a system that consists only of SiC and heavily doped silicon, respectively. We see that in the SiC coated system, the SiC coating contributes significantly in the large wavevector range [as noted by comparing Figs. 7(a) and 7(b)], whereas the heavily doped silicon provides significant contribution to the heat transfer in the lower wavevector range and over a broad frequency range [as noted by comparing Figs. 7(a) and 7(c)]. The combination of significant contributions of both the SiC thin film and the bulk heavily doped silicon region results in the significant enhancement of exergy in this system.

IV. CONCLUSIONS

We have provided conditions for achieving maximal exergy in the near-field heat transfer between planar bodies. A closed-form formula of exergy allowed us to derive the conditions of parameters of the system for maximizing the exergy. These conditions, in particular, indicate that there exists an optimal choice of the resonant linewidth γ. The analytical formulas of exergy and the optimal conditions were verified by the fluctuational electrodynamics calculations. We also show that the theoretical conditions can be used to guide the design of practical structures for maximizing exergy. In particular, in the heavily doped silicon system, we have shown that the exergy can be enhanced by tuning the doping concentration. In addition, by considering a combined system where a thin SiC layer is placed on top of heavily doped silicon, significant further enhancement of the exergy can be obtained, comparing with a typical phonon-polariton system with similar resonant frequencies, since the combined system has a loss characteristic that is closer to the optimal condition. Our results provide a fundamental understanding and design guideline for maximizing the exergy in heat transfer on the nanoscale and point to significant opportunities for either controlling material or meta-material properties or enhancing the performance of thermal energy conversion.

ACKNOWLEDGMENTS

Professor Fan's contribution to this publication was as a consultant and was not part of his Stanford duties or responsibilities.

[1]P. T. Landsberg and G. Tonge, J. Appl. Phys. **51**, R1 (1980).
[2]P. T. Landsberg and P. Baruch, J. Phys. A: Math. Gen. **22**, 1911 (1989).
[3]A. De Vos, P. T. Landsberg, P. Baruch, and J. E. Parrott, J. Appl. Phys. **74**, 3631 (1993).
[4]C. Zamfirescu and I. Dincer, J. Appl. Phys. **105**, 044911 (2009).
[5]A. Narayanaswamy and Y. Zheng, Phys. Rev. B **88**, 075412 (2013).
[6]I. Latella, A. Perez-Madrid, L. C. Lapas, and J. M. Rubi, J. Appl. Phys. **115**, 124307 (2014).
[7]I. Latella, A. Perez-Madrid, J. M. Rubi, S.-A. Biehs, and P. Ben-Abdallah, Phys. Rev. Appl. **4**, 011001 (2015).
[8]A. Narayanaswamy and G. Chen, Appl. Phys. Lett. **82**, 3544 (2003).
[9]M. Laroche, R. Carminati, and J.-J. Greffet, J. Appl. Phys. **100**, 063704 (2006).
[10]K. Park, S. Basu, W. P. King, and Z. M. Zhang, J. Quant. Spectrosc. Radiat. Transfer **109**, 305 (2008).
[11]S. Basu, Z. M. Zhang, and C. J. Fu, Int. J. Energy Res. **33**, 1203 (2009).
[12]M. Francoeur, R. Vaillon, and M. P. Menguc, IEEE Trans. Energy Convers. **26**, 686 (2011).
[13]O. Ilic, M. Jablan, J. D. Joannopoulos, I. Celanovic, and M. Soljacic, Opt. Express **20**, A366 (2012).
[14]S. Molesky and Z. Jacob, Phys. Rev. B **91**, 205435 (2015).
[15]K. Chen, P. Santhanam, and S. Fan, Appl. Phys. Lett. **107**, 091106 (2015).
[16]M. P. Bernardi, O. Dupre, E. Blandre, P.-O. Chapuis, R. Vaillon, and M. Francoeur, Sci. Rep. **5**, 11626 (2015).

[17]T. J. Bright, L. P. Wang, and Z. M. Zhang, J. Heat Transfer **136**, 062701 (2014).
[18]J. K. Tong, W.-C. Hsu, Y. Huang, S. V. Boriskina, and G. Chen, Sci. Rep. **5**, 10661 (2015).
[19]C. Simovski, S. Maslovski, I. Nefedov, and S. Tretyakov, Opt. Express **21**, 14988 (2013).
[20]J. Y. Chang, Y. Yang, and L. Wang, Int. J. Heat Mass Transfer **87**, 237 (2015).
[21]T. Ikeda, K. Ito, and H. Iizuka, J. Appl. Phys. **121**, 013106 (2017).
[22]R. Messina and P. Ben-Abdallah, Sci. Rep. **3**, 1383 (2013).
[23]V. B. Svetovoy and G. Palasantzas, Phys. Rev. Appl. **2**, 034006 (2014).
[24]M. Lim, S. Jin, S. S. Lee, and B. J. Lee, Opt. Express **23**, A240 (2015).
[25]D. Polder and M. Van Hove, Phys. Rev. B **4**, 3303 (1971).
[26]J. B. Pendry, J. Phys.: Condens. Matter **11**, 6621 (1999).
[27]K. Joulain, J.-P. Mulet, F. Marquier, R. Carminati, and J.-J. Greffet, Surf. Sci. Rep. **57**, 59 (2005).
[28]D. G. Cahill, P. V. Braun, G. Chen, D. R. Clarke, S. Fan, K. E. Goodson, P. Keblinski, W. P. King, G. D. Mahan, A. Majumdar, H. J. Maris, S. R. Phillpot, E. Pop, and L. Shi, Appl. Phys. Rev. **1**, 011305 (2014).
[29]E. Rousseau, A. Siria, G. Jourdan, S. Volz, F. Comin, J. Chevrier, and J.-J. Greffet, Nat. Photonics **3**, 514 (2009).
[30]S. Shen, A. Narayanaswamy, and G. Chen, Nano Lett. **9**, 2909 (2009).
[31]K. Kim, B. Song, V. Fernandez-Hurtado, W. Lee, W. Jeong, L. Cui, D. Thompson, J. Feist, M. T. Homer Reid, F. J. Garcia-Vidal, J. C. Cuevas, E. Meyhofer, and P. Reddy, Nature **528**, 387 (2015).
[32]L. Hu, A. Narayanaswamy, X. Chen, and G. Chen, Appl. Phys. Lett. **92**, 133106 (2008).
[33]R. S. Ottens, V. Quetschke, S. Wise, A. A. Alemi, R. Lundock, G. Mueller, D. H. Reitze, D. B. Tanner, and B. F. Whiting, Phys. Rev. Lett. **107**, 014301 (2011).
[34]R. St-Gelais, B. Guha, L. Zhu, S. Fan, and M. Lipson, Nano Lett. **14**, 6971 (2014).
[35]K. Ito, A. Miura, H. Iizuka, and H. Toshiyoshi, Appl. Phys. Lett. **106**, 083504 (2015).
[36]A. Kittel, W. Muller-Hirsch, J. Parisi, S.-A. Biehs, D. Reddig, and M. Holthaus, Phys. Rev. Lett. **95**, 224301 (2005).
[37]Y. De Wilde, F. Formanek, R. Carminati, B. Gralak, P.-A. Lemoine, K. Joulain, J.-P. Mulet, Y. Chen, and J.-J. Greffet, Nature **444**, 740 (2006).
[38]B. Guha, C. Otey, C. B. Poitras, S. Fan, and M. Lipson, Nano Lett. **12**, 4546 (2012).
[39]J. B. Pendry, A. J. Holden, W. J. Stewart, and I. Youngs, Phys. Rev. Lett. **76**, 4773 (1996).
[40]L. Solymar and E. Shamonina, *Waves in Metamaterials* (Oxford University, New York, 2009).
[41]S. Basu, B. J. Lee, and Z. M. Zhang, J. Heat Transfer **132**, 023301 (2010).
[42]H. Iizuka and S. Fan, Phys. Rev. B **92**, 144307 (2015).
[43]I. W. Boyd, T. D. Binnie, J. I. B. Wilson, and M. J. Colles, J. Appl. Phys. **55**, 3061 (1984).
[44]D. Olego and M. Cardona, Phys. Rev. B **25**, 3889 (1982).
[45]A. Herve, J. Drevillon, Y. Ezzahri, K. Joulain, D. D. S. Meneses, and J.-P. Hugonin, J. Quant. Spectrosc. Radiat. Transfer **180**, 29 (2016).